ACS OMEGA

Open Access

http://pubs.acs.org/journal/acsodf

Article

Molecular-Level Interactions in Binary Mixtures of 1-Ethyl-3-methylimidazolium Ethylsulfate and Propane-1,2-diol: The Interplay between Intermolecular and Intramolecular Hydrogen Bonding

Md. Ahad Ali and Md. Abu Bin Hasan Susan*

Cite This: *ACS Omega* 2023, 8, 32690−32700

Read Online

ACCESS | Metrics & More | Article Recommendations | Supporting Information

ABSTRACT: In this study, volumetric properties of an ionic liquid, 1-ethyl-3-methylimidazolium ethylsulfate ($[C_2mim]C_2H_5SO_4$), propane-1,2-diol, and their binary mixtures were studied by measurements of density and viscosity. The excess molar volume (V_m^E), dynamic viscosity deviation ($\Delta\eta$), and excess molar Gibbs free energy of activation for viscous flow (ΔG_m^*) were calculated and fitted with the Redlich−Kister (RK) type polynomial equation. The results suggested that intermolecular interactions are weaker in the mixture compared to the pure components and the interactions decrease with increasing mole fraction of $[C_2mim]C_2H_5SO_4$. The thermodynamic activation parameters were also calculated from the Eyring equation, and their variations with mole fraction of $[C_2mim]C_2H_5SO_4$ were correlated to the molecular-level interactions. The near-infrared (NIR) spectroscopic measurements were carried out in the temperature range from 293.15 to 333.15 K. The raw NIR data were analyzed further by two-dimensional correlation spectroscopy and principal component analysis. When $[C_2mim]C_2H_5SO_4$ was introduced to the propane-1,2-diol system, the stronger intermolecular hydrogen bonds were destroyed. Propane-1,2-diol and $[C_2mim]C_2H_5SO_4$ produce some weaker hydrogen bonds, but the effect of breaking hydrogen bonds predominates. On the basis of volumetric and NIR spectroscopic investigations, molecular-level interactions are predicted. The interplay between intermolecular and intramolecular hydrogen bonding decides unique molecular-level interactions and dictates enhanced thermodynamic properties of the binary mixtures to make them tunable for a multitude of applications.

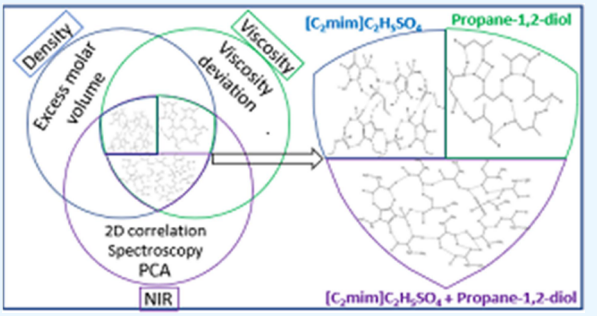

INTRODUCTION

Ionic liquids (ILs) are one of the most intriguing breakthroughs in solvent chemistry. The terminology "ILs" alludes to solvent materials that are only composed of ions but are liquids below 373.15 K. ILs received an upsurge of interest because of their eco-friendly characteristics and superior physicochemical properties which include relatively low melting point, non-flammability, imperceptible vapor pressure, wide electrochemical window, high electrical conductivity, immense thermal stability, wide liquidous range, a great capacity of dissolving a variety of inorganic and organic substances, and even the flexibility of tailoring the structure of cations and anions to get optimum physicochemical properties.[1,2] These extraordinary properties have made ILs pragmatic in industries as electrolytes in modern energy devices, solvents in chemical reactions,[3,4] extraction,[5,6] separation,[7,8] electrodeposition,[9] medium of nanomaterial synthesis,[10,11] enzyme catalysis,[12,13] and gas capture.[14]

Despite a number of superior features of ILs over conventional organic solvents, their applications have become dwindled because of their extravagant nature and erratic properties like high viscosity, hygroscopic nature, etc.[15] However, the prospect of tuning the properties by tailoring the ions retained the hope of overcoming the problems. Tokuda et al., through their systematic study of aprotic ILs, established that their physicochemical properties depend on their structural components and may be altered by manipulating the constituent cation, anion, and sub-constituent alkyl chain proportions.[16−18] They utilized the effective ion contribution and the amount of force balance between multiple interacting forces to characterize the transformations of physicochemical characteristics. Another way of adjustment of physicochemical properties is the preparation of binary mixtures of ILs with conventional molecular solvents. Pereiro et al. calculated excess molar volumes, changes in refractive indices upon mixing, and isentropic compressibility from measurements of densities, sound velocities, and refractive indices of binary mixtures of ethanol with 1,3-dimethylimidazolium methylsulfate, 1-butyl-3-methylimidazolium methylsul-

Received: May 18, 2023
Accepted: July 14, 2023
Published: August 30, 2023

Table 1. Densities and Dynamic Viscosities of $[C_2mim]C_2H_5SO_4$ and Propane-1,2-diol and Their Comparison with Literature Values at 298.15 K

compound	ρ (g cm^{-3})		η (mPa s)	
	experimental	literature	experimental	literature
$[C_2mim]C_2H_5SO_4$	1.23617	1.23635[33]	96.024	96.21[39]
		1.23763[34]		97.58[34]
		1.23670[35]		97.2[40]
propane-1,2-diol	1.03333	1.03262[36]	42.131	45.440[38]
		1.03258[37]		43.661[37]
		1.0331[38]		43.437[41]

fate, 1-butyl-3-methylimidazolium hexafluorophosphate, 1-hexyl-3- methylimidazolium hexafluorophosphate, and 1-methyl-3-octylimidazonium hexafluorophosphate at T = 293.15 to 303.15 K.[19] AlTwaim et al. investigated the impact of alkyl chain length on the physical characteristics of binary mixtures of propane-1-ol, butane-1-ol, and pentane-1-ol with 1-ethyl-3-methylimidazolium methylsulfate. They measured the viscosities and surface tensions and calculated the corresponding deviation properties and excess Gibbs free energy using the experimental data.[20]

Physicochemical properties of the binary mixtures of $[C_2mim]C_2H_5SO_4$ with molecular organic solvents including water, methane-1-ol, ethane-1-ol, propane-1-ol, propane-2-ol, acetone, acetonitrile, propylene carbonate, dichloromethane, and sugars are available in the literature. Miaja et al. reported the density data of binary mixtures of $[C_2mim]C_2H_5SO_4$ with water,[21] Gonza'lez et al. reported the densities, velocities of sound, and refractive indices of binary mixtures of $[C_2mim]$-$C_2H_5SO_4$ with methane-1-ol, propane-1-ol, and propane-2-ol.[22] Lehmann et al. reported the density data of binary mixtures of $[C_2mim]C_2H_5SO_4$ with acetone, acetonitrile, propylene carbonate, dichloromethane, methanol, ethanol, and water.[23] Kiefer et al. investigated molecular-level interaction between $[C_2mim]C_2H_5SO_4$ and acetone analyzing peak shifting induced by acetone and the excess infrared (IR) spectra of IL. They showed that rather than interacting with ion pairs, acetone forms hydrogen bonds with the hydrogen of the imidazolium ring.[24] Reddy et al. predicted molecular-level interactions of the binary mixtures of $[C_2mim]C_2H_5SO_4$ and 2-methoxyethanol using both thermodynamic and IR spectroscopic studies.[25]

Volumetric and viscometric studies of a series of dialkyl- and trialkyl-substituted imidazolium-based ILs having $[NTF_2]$ anion with a series of molecular solvents like ethylene glycol, diethylene glycol dimethylether, triethylene glycol dimethylether, etc.[26−28] and volumetric properties and spectroscopic studies of binary mixtures of various ammonium- and imidazolium-based ILs with a series of alcohols were used to predict molecular-level interactions.[29−31]

Near-infrared (NIR) spectroscopy has been extensively used to investigate molecule-level interactions in binary mixtures of many ILs and molecular solvents. The binary mixtures of ILs not only improve the properties of the medium for task-specific applications but also reduce the expense. Alcohols with −OH groups in the structure are susceptible to hydrogen bonding and hence have immense prospects for tuning the physicochemical properties. We intend to use NIR spectroscopy to gain a qualitative and quantitative understanding of the interactions between the numerous hydrogen-bonded species present in binary mixtures of $[C_2mim]C_2H_5SO_4$ with alcohols. We have already reported the molecular-level interactions between $[C_2mim]C_2H_5SO_4$ and a monohydric alcohol, propane-1-ol, and observed that when the IL is added to propane-1-ol owing to the fewer hydrogen bonding sites the intermolecular hydrogen bonds easily undergo disruption and solvate the ions to yield negative values of excess thermodynamic properties.[32] It is a burgeoning question, whether an alcohol with multiple −OH groups in the structure exhibit similar behavior and influence physicochemical properties in an identical fashion. To gain a deep insight, it is, therefore, crucial to understand molecular-level interactions of the IL with a dihydric alcohol and compare and contrast with a monohydric alcohol in terms of enhancement of thermodynamic properties of the binary mixtures. In this study, we used $[C_2mim]C_2H_5SO_4$, propane-1,2-diol, and their binary mixtures for a detailed analysis. The variations in excess molar volumes, dynamic viscosity deviations, and excess molar Gibbs free energy of activation for the viscous flow of binary mixtures with composition have been explained using spectroscopic observations to develop a fundamental knowledge-base on interaction in the molecular-level and consequent enhancement in thermodynamic properties for systems of this kind.

EXPERIMENTAL SECTION

The IL, $[C_2mim]C_2H_5SO_4$ obtained from Merck at ≥95% purity, was used after vacuum drying and the water content was found 1.027 wt % in the ambient condition determined by the Karl-Fischer titrator (Metrohm 860-KF). The propane-1,2-diol at ≥99.55% purity was obtained from Merck and was used without further purification. The gravimetric method was used to prepare the binary mixtures with the following compositions given in $[C_2mim]C_2H_5SO_4$ mole fraction: 0 (pure propane-1,2-diol), 0.1, 0.2, 0.3, 0.4, 0.5, 0.6, 0.7, 0.8, 0.9, and 1 (pure $[C_2mim]C_2H_5SO_4$).

The measurements of densities and dynamic viscosities were carried out in an Anton Paar (DMA 4500 M) densimeter having a standard deviation of ±0.00001 g cm^{-3} and an Anton Paar (Lovis 2000 ME) microviscometer with a standard deviation of ±0.001 mPa s, respectively, automatically thermostated within ±0.01 K by a built-in Peltier device in the temperature range from 293.15 to 333.15 K with 5 K intervals. A Fourier transform spectrophotometer (FTIR/NIR, PerkinElmer, USA) was used to record the NIR spectra in the range 4000−10,000 cm^{-1} at 2 cm^{-1} resolution. Temperature-dependent NIR spectra of materials were measured using a highly sensitive liquid sampling cell with a pair of rectangular CaF_2 windows with curved edges (Specac model no. GS20522). To keep the path length constant at 0.02 mm, a rectangular polytetrafluoroethylene spacer was used. The mathematical calculations and statistical analyses were done in OriginPro 2019b. Before analysis, the raw NIR data were baseline-corrected. All the mathematical and statistical treat-

https://doi.org/10.1021/acsomega.3c03457
ACS Omega 2023, 8, 32690−32700

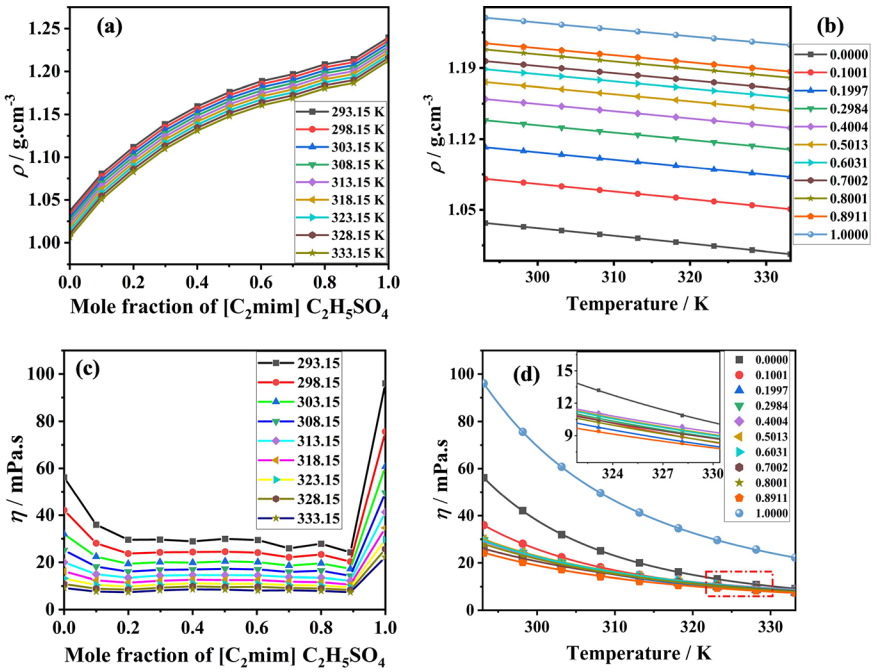

Figure 1. Variation of density with (a) mole fraction of $[C_2mim]C_2H_5SO_4$ and (b) temperature and variation of viscosity with (c) mole fraction (lines are for visual aids only) and (d) temperature for binary mixtures of $[C_2mim]C_2H_5SO_4$ and propane-1,2-diol. (Lines are predicted from the VFT equation.)

ments were performed for the NIR data in the range from 6000 to 7150 cm^{-1}.

RESULTS AND DISCUSSION

The densities and dynamic viscosities of pure $[C_2mim]$-$C_2H_5SO_4$ and propane-1,2-diol were measured along with their binary mixtures over the temperature range from 293.15 to 333.15 K at 5 K intervals. The comparison of the experimental densities and viscosities is tabulated in Table 1.

Density increases with increasing the mole fraction of $[C_2mim]C_2H_5SO_4$ (Figure 1a). This behavior suggests greater packing in mixtures compared to the pure components and the possibility of the presence of ion−dipole interactions between the unlike molecules. At a lower mole fraction of $[C_2mim]$-$C_2H_5SO_4$, the system behaves like a very dilute ionic solution. As the mole fraction of $[C_2mim]C_2H_5SO_4$ increases, the system gradually becomes a concentrated ionic solution with more or less conspicuous ion pairing.[42,43] The changes in density with temperature for the binary mixtures are depicted in Figure 1b. The density decreases with increasing temperature. The molecular movements (translational, rotational, and vibrational) of $[C_2mim]C_2H_5SO_4$ and propane-1,2-diol molecules increase as the temperature rises. As a result, the volumes of binary mixtures and pure components increase the density decreases.

The dynamic viscosity decreases with increasing mole fraction of $[C_2mim]C_2H_5SO_4$ (Figure 1c) due to the weakening of the coulombic force between the cations and anions of $[C_2mim]C_2H_5SO_4$. When the amount of propane-1,2-diol is higher, the intermolecular hydrogen bonding becomes dominant in the system over the coulombic interaction between ions of $[C_2mim]C_2H_5SO_4$.[44] However, when mole fraction of $[C_2mim]C_2H_5SO_4$ is higher than 0.9, viscosity increases again due to the strong interionic interaction between the cations and anions of $[C_2mim]$-$C_2H_5SO_4$. The change in viscosity with temperature is depicted in Figure 1d. The dynamic viscosity reduces as the temperature rises for each binary system, indicating a slow descent structural relaxation. The temperature dependency of viscosity is more pronounced at lower temperatures. The temperature dependencies of binary mixtures were described by standard models. The two-parameter Arrhenius model, the most widely used model, and of the three-parameter models, the Vogel−Fulcher−Tammann (VFT)[45−47] and modified VFT (mVFT)[48] models were also applied to fit the temperature dependence of dynamic viscosity of the binary mixtures and their pure components. The temperature dependence of dynamic viscosity follows all the three models. The fitting parameters calculated from each equation are tabulated in Table S1 along with their correlation coefficient values (R^2).

The excess molar volumes for the binary mixtures are calculated from the following (eq 1):

$$V_m^E = \frac{\sum x_i M_i}{\rho_{mix}} - \sum_{i=2}^{n} \frac{x_i M_i}{\rho_i} \quad (1)$$

The excess molar volumes of the binary mixtures are positive over the whole composition range (Figure 2a). The largest value of the excess molar volume is found at 0.9 $[C_2mim]$-$C_2H_5SO_4$ mole fraction. When $[C_2mim]C_2H_5SO_4$ is added to propane-1,2-diol the intermolecular hydrogen bonds between propane-1,2-diol molecules are broken down thus free volume in the solution increases. Hence, molar volume increases. With temperature, the breaking process of hydrogen bonding is favored hence at higher temperatures, values of excess molar volume become more positive. The data points of excess molar volumes for a binary mixture of $[C_2mim]C_2H_5SO_4$ and propane-1,2-diol were fitted with the RK type polynomial expression (eq 2):[49]

https://doi.org/10.1021/acsomega.3c03457
ACS Omega 2023, 8, 32690−32700

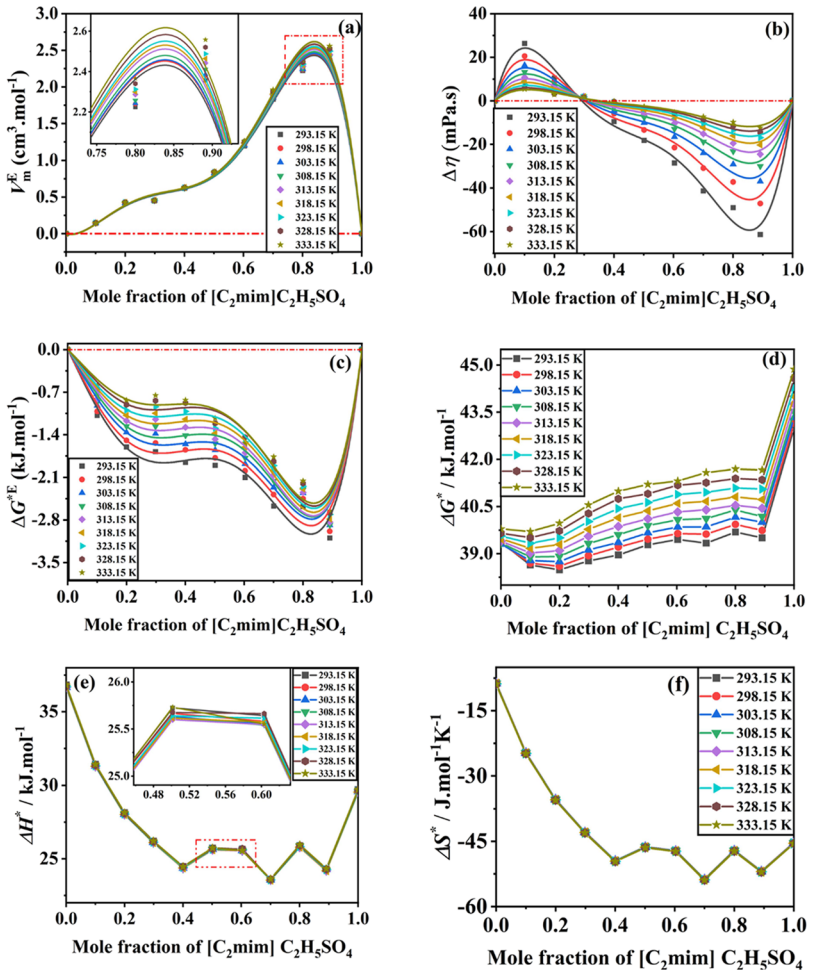

Figure 2. Variation of (a) excess molar volumes, (b) dynamic viscosity deviations, (c) excess molar Gibbs free energy of activation for viscous flow, (d) Gibbs free energy, (e) enthalpy, and (f) entropy of activation for the viscous flow of binary mixtures of $[C_2mim]C_2H_5SO_4$ and propane-1,2-diol as a function of mole fraction of $[C_2mim]C_2H_5SO_4$ at various temperatures.

$$Y^E = x_1x_2\sum_{i=0}^{n} A_i(x_1 - x_2)^i \quad (2)$$

where Y^E is the excess properties, n is the polynomial order, and x_1 and x_2 are the mole fractions of $[C_2mim]C_2H_5SO_4$ and propane-1,2-diol, respectively. A_0−A_n are coefficients of the RK equation calculated by the least-squares type algorithm, which are tabulated in Table S2.

The dynamic viscosity deviations are calculated from the following (eq 3):

$$\Delta\eta = \eta_{experimental} - \sum x_i\eta_i \quad (3)$$

The dynamic viscosity deviations ($\Delta\eta$) for the binary mixture of $[C_2mim]C_2H_5SO_4$ and propane-1,2-diol are positive up to 0.3 mole fraction of $[C_2mim]C_2H_5SO_4$ and negative with increasing mole fraction of $[C_2mim]C_2H_5SO_4$ (Figure 2b). When the amount of $[C_2mim]C_2H_5SO_4$ in the mixture is smaller, the intermolecular hydrogen bonds between propane-1,2-diol molecules are more prominent than the intermolecular interaction with unlike molecules. When the temperature is increased, the $\Delta\eta$ becomes more positive.

At a mole fraction of $[C_2mim]C_2H_5SO_4$ higher than 0.3, the intermolecular ions of $[C_2mim]C_2H_5SO_4$ become solvated resulting from the simultaneous breaking of homomolecular hydrogen bonds between propane-1,2-diol molecules and the formation of less strong heteromolecular interaction between $[C_2mim]C_2H_5SO_4$ and propane-1,2-diol. Hence, the value of $\Delta\eta$ decreases. The $\Delta\eta$ becomes more negative with increasing temperature. Because when temperature increases, the intermolecular attraction decreases; hence, $\Delta\eta$ also decreases. The data points of $\Delta\eta$ are fitted in eq 1. The coefficients of the RK-type expression are tabulated in Table S2.

The excess molar Gibbs free energy for the viscous flow (ΔG^{*E}) of the binary mixtures are calculated from the following (eq 4):

$$\Delta G^{*E} = RT[\ln\left(\frac{\eta V}{\eta_2 V_2}\right) - x_1\ln\left(\frac{\eta_1 V_1}{\eta_2 V_2}\right)] \quad (4)$$

The ΔG^{*E} of the binary mixture of $[C_2mim]C_2H_5SO_4$ and propane-1,2-diol are unsymmetrical and all negative over the whole composition range (Figure 2c). The values of the ΔG^{*E} are more negative at higher $[C_2mim]C_2H_5SO_4$ content because of the smaller number of hydrogen bonds present in the system.[50−52] The data points of ΔG^{*E} are fitted in eq 1. The coefficients of the RK-type expression are tabulated in Table S2. Activation enthalpy (ΔH^*) and entropy (ΔS^*) for viscous flow were calculated from the Eyring theory using the following (eq 5):

https://doi.org/10.1021/acsomega.3c03457
ACS Omega 2023, 8, 32690−32700

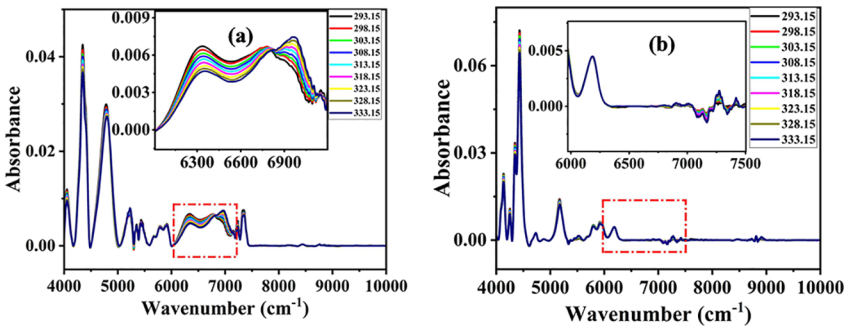

Figure 3. NIR spectra of (a) pure propane-1,2-diol and (b) $[C_2mim]C_2H_5SO_4$ at temperatures from 293.15 to 313.15 K at 5 K intervals.

$$\eta = \frac{hN_A}{V} e^{(\Delta H^*/RT - \Delta S^*/R)} \quad (5)$$

From the values of ΔH^* and ΔS^*, the activation Gibbs free energy was calculated from the following (eq 6):

$$\Delta G^* = \Delta H^* - T\Delta S^* \quad (6)$$

The values of activation parameters for the binary mixture of $[C_2mim]C_2H_5SO_4$ and propane-1,2-diol are summarized in Table S3, respectively, along with R^2 values.

The values of ΔG^* are all positive over the whole composition range (Figure 2d). The positive values of ΔG^* indicate that activation processes for viscous flow are non-spontaneous and molecules absorb energy to perform useful work. The value of ΔG^* increases slightly with increasing mole fraction of $[C_2mim]C_2H_5SO_4$ up to 0.85 and the change of ΔG^* is very small at a lower mole fraction of $[C_2mim]$-$C_2H_5SO_4$ up to 0.85 and then increases abruptly in the pure component. As discussed earlier, the ΔG^* controls fluid flow, which is governed by the ability of the molecules and/or ions to move into a structural hole and the capability to create another hole. The increase in the ΔG^* value indicates an increasing amount of intermolecular attraction forces between the unlike molecules. The values of ΔS^* are all negative over the whole composition range (Figure 2e). At a lower mole fraction of $[C_2mim]C_2H_5SO_4$, the entropy decreases indicating that the addition of $[C_2mim]C_2H_5SO_4$ in liquid propane-1,2-diol makes the system more ordered. However, at higher mole fractions, the entropy change fluctuates indicating the breaking of the hydrogen bond between propane-1,2-diol and the reformation of the solvation cage depending on the number of ions present in propane-1,2-diol. The binary mixtures with mole fractions 0.4, 0.7, and 0.9 have the lowest values that indicate structures of these mixtures are the most ordered structures. The positive values of ΔH^* over the whole composition range at each temperature (Figure 2f) indicate that the mixing of $[C_2mim]C_2H_5SO_4$ in propane-1,2-diol is an endothermic process. The values of ΔH^* decrease up to a 0.4 mole fraction of $[C_2mim]C_2H_5SO_4$, and fluctuation of ΔH^* occurs with more amount of $[C_2mim]C_2H_5SO_4$. The reason for decreasing the value of ΔH^* is that the propane-1,2-diol structure is highly interconnected with the number of intermolecular and intramolecular bonds. However, when $[C_2mim]C_2H_5SO_4$ is added to it, some of the bonds are broken down creating a substantial amount of energy, which lowers the value of ΔH^*.

Hence, by considering the above thermodynamic activation parameters, at a lower mole fraction of $[C_2mim]C_2H_5SO_4$ up to 0.4, the intermolecular interactions between the like propane-1,2-diol molecules decrease via intermolecular and intramolecular hydrogen bond breaking along with solvation of $[C_2mim]C_2H_5SO_4$ by propane-1,2-diol molecules. Further, the addition of $[C_2mim]C_2H_5SO_4$ creates the shortage of propane-1,2-diol in the system for solvation to occur, and then there is a competition between intermolecular forces between like molecules of $[C_2mim]C_2H_5SO_4$ and propane-1,2-diol. It is in sharp contrast to $[C_2mim]C_2H_5SO_4$/propane-1-ol binary system, where due to the less number of hydrogen bonding sites the intermolecular hydrogen bonds easily break down and solvate the ions when $[C_2mim]C_2H_5SO_4$ is added to propane-1-ol, hence excess thermodynamic properties are negative,[32] but in case of the $[C_2mim]C_2H_5SO_4$/propane-1,2-diol system, the excess thermodynamic parameters are positive due to the stronger intermolecular association of propane-1,2-diol molecules by forming more hydrogen bonding network.

The NIR spectroscopic measurements were carried out for pure propane-1,2-diol and $[C_2mim]C_2H_5SO_4$ at the temperature range from 293.15 to 333.15 K at a 5 K intervals. The NIR spectra are depicted in Figure 3. In NIR spectra of propane-1,2-diol, numbers of peaks are present in the range between 6000 and 7150 cm^{-1}. The peaks in this region are assigned as peaks of the first overtone band of −OH stretching vibration for −OH bonds in different electronic environments.[53,54]

The peak at 7016 cm^{-1} is assigned to the −OH group, which is hydrogen bond acceptors only and the peak at 7100 cm^{-1} is for non-hydrogen-bonded free −OH groups.[55] As the temperature increases, the intensity of absorbance for the band at 7050 cm^{-1} increases, and at a higher temperature, it becomes sharp suggesting that with increasing temperature number of intermolecular hydrogen bonds decreases. Besides, the intensity of peak at 7050 cm^{-1} also increases with temperature, indicating that at higher temperatures, some of the intermolecular hydrogen bonds break down to form free propane-1,2-diol.

The peaks at 6300 and 6800 cm^{-1} are for cooperative intermolecular and intramolecular and non-cooperative intermolecular and intramolecular hydrogen-bonded −OH groups, respectively.[46] The decrease in intensity of these bands also suggests the presence of a higher number of hydrogen-bonded −OH groups in the different molecular environments. There exists an isosbestic point at 6720 cm^{-1}. In the NIR spectra of $[C_2mim]C_2H_5SO_4$, there is only one broad peak at 6200 cm^{-1} that remains unchanged with temperature. This peak comes from the second overtone of −CH stretching.

The temperature-perturbed 2D correlation spectral analysis of propane-1,2-diol in the temperature range 293.15 to 333.15 K from 6000 to 7150 cm^{-1} was performed for the raw spectral

https://doi.org/10.1021/acsomega.3c03457
ACS Omega 2023, 8, 32690−32700

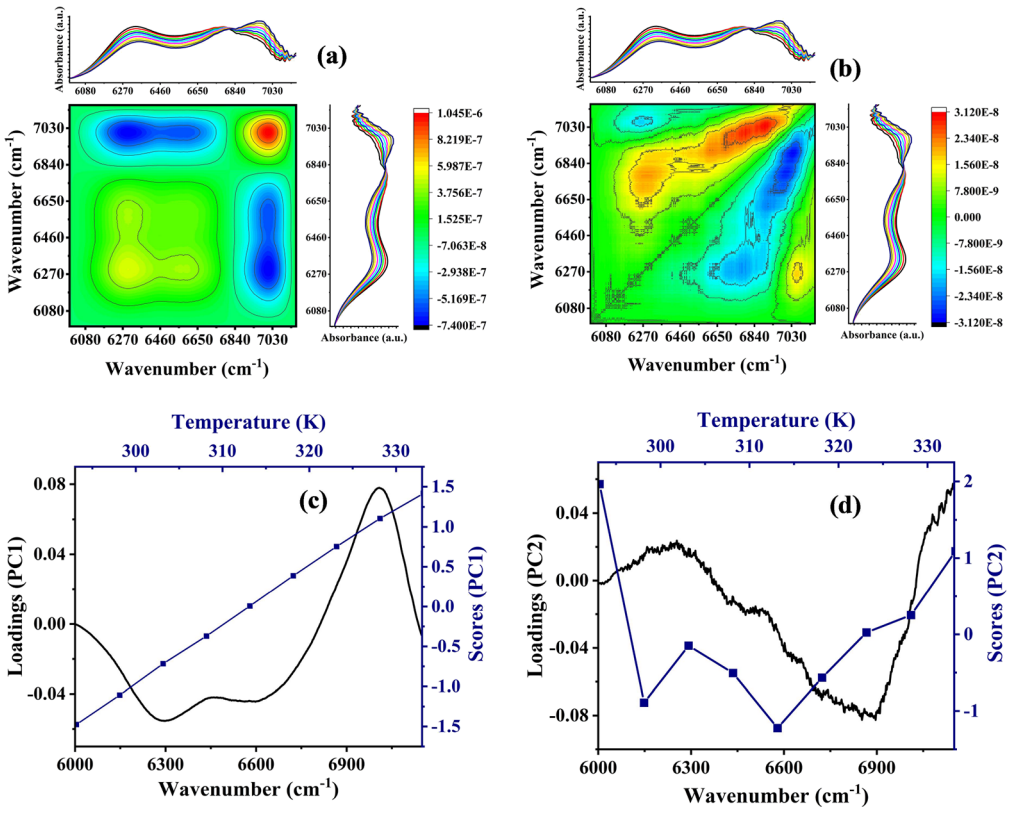

Figure 4. (a) Synchronous and (b) asynchronous 2D NIR correlation spectra and loadings and scores (c) PC1 and (d) PC2 calculated from the temperature-dependent spectral changes (293.15 to 313.15 K) of pure propane-1,2-diol.

data. Figure 4 shows the synchronous and asynchronous spectra of the 2D correlation analysis of propane-1,2-diol in the region of 6000−7150 cm^{-1}.

The synchronous 2D NIR correlation spectrum shows two major diagonal auto peaks. The auto peak at 6300 cm^{-1} is for the hydrogen-bonded O-H bond. However, the auto peak at 7016 cm^{-1} has high correlation intensity (more than 10 times that of the peak at 6300 cm^{-1}). This suggests that in propane-1,2-diol, the intermolecular hydrogen bonds are present but most of the O-H bonds are hydrogen bond acceptors, and also a smaller number of the free hydroxyl groups are present in the propane-1,2-diol system.

The negative cross-peaks between these auto peaks suggest that spectral changes at these positions are negatively correlated to each other. In addition, since the cross-peak of 6300 and 7016 cm^{-1} in the asynchronous map is negative, the variance at 6300 cm^{-1} occurs at higher temperatures compared to that at 7016 cm^{-1}. According to the principle of 2D correlation spectra, as the temperature rises, the vibration at 6300 cm^{-1} transforms into the vibration at 7016 cm^{-1}. To verify and quantify the results of 2D correlation spectra, principal component analysis (PCA) was done for propane-1,2-diol in the same temperature and wavenumber range of the 2D correlation. The PCA of propane-1,2-diol gives nine principal components, then the first two components dominated over 99.94173% of the total system. The other seven components have very little contribution to the total spectra. The eigenvalues and percentage of variance for the principal components of propane-1,2-diol are given in Table 2.

The loading of the PC1 shows a broad peak at 6300 cm^{-1}, with a significant shoulder at 6600 cm^{-1} (Figure 4c), signifies the presence of a hydrogen-bonded cluster dominated by this

Table 2. Eigenvalues and Percentage of Variance for the Principal Components of Propane-1,2-diol

principal components	eigen values	percentage of variance	cumulative percentage
1	1.71285×10^{-4}	99.57482	99.57482
2	6.31134×10^{-7}	0.3669	99.94173
3	4.71752×10^{-8}	0.02742	99.96915
4	2.38761×10^{-8}	0.01388	99.98303
5	1.33195×10^{-8}	0.00774	99.99077
6	7.45778×10^{-9}	0.00434	99.99511
7	5.39172×10^{-9}	0.00313	99.99824
8	3.01935×10^{-9}	0.00176	100
9	1.16175×10^{-34}	6.75368×10^{-29}	100

principal component. In addition, there is a negative peak at 7016 cm^{-1} which corresponds to the auto peak and cross-peaks of 2D correlation spectra, respectively. The scores of this principal component decrease with increasing temperature. In the case of PC2 in the hydrogen-bonded region, there is no significant peak rather stronger peaks at 7100 cm^{-1} and higher wavenumbers (Figure 4d). This signifies PC2 is predominantly non-hydrogen-bonded propane-1,2-diol. The scores of PC2 decrease first and then increase with increasing temperature. As the temperature rises, hydrogen-bonded clusters of propane-1,2-diol begin to break down to form non-hydrogen-bonded free propane-1,2-diol molecules.

The NIR spectra of the prepared binary mixtures were recorded over a temperature range from 293.15 to 333.15 K at a 5 K intervals. For pure propane-1,2-diol, the presence of two broad peaks in the region between 6200 to 7000 cm^{-1} suggests the presence of different types of clusters in the pure propane-

https://doi.org/10.1021/acsomega.3c03457
ACS Omega 2023, 8, 32690−32700

1,2-diol system.[16] However, when $[C_2mim]C_2H_5SO_4$ is added to it, some of the structural modification occurs that reflects in the shifting of the bands and change in their intensities. At 0.1 $[C_2mim]C_2H_5SO_4$ mole fraction, the broad peak at 6200 cm^{-1} undergoes a blueshift suggesting the weakening of the strength of hydrogen bonds between the molecules. As the peak at 6200 cm^{-1} is for the doubly hydrogen-bonded species, it can be predicted that one of the two hydrogen bonds weakened due to the effect of $[C_2mim]C_2H_5SO_4$. The redshift of the peak in the region of 6932 cm^{-1} suggests the strengthening of the intramolecular hydrogen bonding in the propane-1,2-diol molecule. This is due to the fact that when one of the two hydrogen bonds becomes weaker, the other one becomes stronger. As the intermolecular hydrogen bonds become weaker due to the addition of $[C_2mim]C_2H_5SO_4$, the intramolecular bonds become stronger. Another new peak observed in the region of 6800 cm^{-1} suggests the inclusion of a new type of species containing weak hydrogen bonding interaction. Surprisingly, the peak at 7080 and 7016 cm^{-1} is absent for the 0.1 $[C_2mim]C_2H_5SO_4$ mole fraction binary system suggesting that the free −OH groups are engaged with any of the hydrogen bonding interaction.

The 2D synchronous contour map shows a strong auto peak at 7016 cm^{-1} and broader and weaker auto peaks at 6332 and 6594 cm^{-1}, respectively (Figure S1). These auto peaks suggest a strong correlation between the peaks. The off-diagonal negative cross-peaks between 7016 and 6594 cm^{-1} and between 7016 and 6332 cm^{-1} suggest that these peaks are negatively correlated with one another. The asynchronous contour map also shows a strong negative correlation between the peak at 7016 cm^{-1} and the peaks at 6332 and 6594 cm^{-1} (Figure S1). It is evident that the broad peak at 6932 cm^{-1} is composed of at least two peaks at 6594 and 7016 cm^{-1}.

For further quantitative analysis, PCA is done for this spectral data (Table S4). The first principal component PC1 contributes to 66.29023% of the total spectral variance and has loadings that are dominated by broad negative peaks between 6200 and 6900 cm^{-1} and a positive peak at 7016 cm^{-1}, which indicates the presence of negatively correlated peaks in this species (Figure S2). The scores are increasing with increasing temperature. At lower temperature, clusters of PC1 contains more doubly hydrogen-bonded species, and at increasing temperature, this species is partially broken down to form a single hydrogen-bonding-accepting species. The loadings of the second principal component, PC2, which have a 31.69037% contribution to the total spectral variance, show the presence of a single positive peak centering at 7000 cm^{-1}, and the positive scores are found at temperatures 293.15, 303.15, 318.15, and 333.15 K. In other temperatures, the scores are negative. This fluctuation indicates the existence of several temperatures that change the spectral features. The shape of the peak at 7000 cm^{-1} indicates the presence of two or more peaks inside this. The two shoulders at the left and right side of this peak indicate that there exists some free −OH.

At 0.2 $[C_2mim]C_2H_5SO_4$ mole fraction, the peak at 6184 cm^{-1} due to the second overtone of the C−H stretching vibration for C−H of the imidazolium ring becomes more intense and separable, but the intensity of the peaks for strongly hydrogen-bonded O−H vibrations becomes less intense. A broad peak at 7000 cm^{-1} is also found similar to that of 0.1 $[C_2mim]C_2H_5SO_4$ mole fraction. The 2D correlation synchronous contour map of this binary mixture gives strong auto peaks at 7016 and 6320 cm^{-1} (Figure S3). The negative cross-peaks between these two peaks suggest that these two peaks are negatively correlated to each other. The peak at 6320 cm^{-1} is divergent to the off-diagonal position suggesting the presence of more bonds inside this region. These more bonds are for different types of hydrogen bonds present in this system. The difference between the spectrum of 0.1 and 0.2 $[C_2mim]C_2H_5SO_4$ mole fraction is in the broadness of the auto peaks. The broader auto peak for the latter system suggests more peak shifting. The PC1 has a variance value of 62.98869% and contains two positive peaks at 6184 and 6520 cm^{-1} (Table S5). The scores show an almost constant value near zero from temperature 298.15 to 328.15 K, but, at 333.15 K, the scores become negative indicating a sharp spectral variation of PC1 at this temperature (Figure S4). The PC2 for this is the same as PC2 of 0.1$[C_2mim]C_2H_5SO_4$ mole fraction in the mixture. The only difference is in the scores. Whereas the scores for the former mixture were fluctuating, the scores for the latter one increase linearly with temperature. The loadings of PC3 give a negative peak at 6184 cm^{-1} and a broad positive peak at 6750 cm^{-1}. The scores at 303.15 K temperature show a sharp decrease in the score value. The most interesting feature of all the principal components for this particular binary system is that at 303.15 K there is a sharp change in score.

For $[C_2mim]C_2H_5SO_4$ mole fraction of 0.3 in the mixture, the peak at 6184 cm^{-1} becomes more resolved and the peak at 6332 cm^{-1} becomes vanished. This is because when $[C_2mim]$-$C_2H_5SO_4$ is added to propane-1,2-diol, the intermolecular stronger hydrogen bonds are broken down and new weaker hydrogen bonds are formed between unlike molecules. The blueshift of the peaks at 6900 cm^{-1} gives further evidence of this occurrence. The synchronous 2D correlation contour plot of this binary system has three major auto peaks at 6672 and 7016 cm^{-1} (Figure S5). Besides these major peaks, there is a minor auto peak at 6184 cm^{-1}. The negative correlations between the peaks at 6672 and 7016 cm^{-1}, 6194, and 6672 cm^{-1} are confirmed by the presence of negative cross-peaks. The positive cross-peaks between 6184 and 7016 cm^{-1} show that there is a positive correlation between these peaks. Hence, at 0.3 $[C_2mim]C_2H_5SO_4$ mole fraction, as the temperature increases the hydrogen bonds break down and form weaker hydrogen-bonded species. Positive correlation between the peaks for 6184 and 7016 cm^{-1} shows that the inclusion of $[C_2mim]C_2H_5SO_4$ in propane-1,2-diol increases the probability of finding clusters with the weakly hydrogen-bonded −OH group. Loadings of PC1 that have a 73.86322% contribution to the total spectral variation give weak positive peaks at 6184 and 7016 cm^{-1} and negative peaks at 6332 and 6672 cm^{-1} (Table S6). The scores of PC1 give a sharp increase at 308.15 K and then become mostly unchanged up to 328.15 K (Figure S6). This observation shows that the contribution of PC1 in spectral variation has some significant variation at 308.15 K. The loadings of peaks suggest that PC1 is mainly imidazolium cations solvated with propane-1,2-diol via weak hydrogen bonds and some of the −OH groups are intramolecularly hydrogen-bonded also. The loadings of PC2 have a sharp peak at 6998 cm^{-1}. There are some noises in the hydrogen bonding overtone region. Therefore, the PC2 is mainly the component where majorly propane-1,2-diol are found of which a very small number of weak hydrogen bonds are found.

https://doi.org/10.1021/acsomega.3c03457
ACS Omega 2023, 8, 32690−32700

Scheme 1. Schematic Diagram of Molecular-Level Interaction of (a) Pure Propane-1,2-diol, (b) Pure $[C_2mim]C_2H_5SO_4$, (c) Binary Mixture of $[C_2mim]C_2H_5SO_4$ and Propane-1,2-diol When Mole Fraction of Propane-1,2-diol is Greater, and (d) Binary Mixture of $[C_2mim]C_2H_5SO_4$ and Propane-1,2-diol When Mole Fraction of $[C_2mim]C_2H_5SO_4$ is Greater

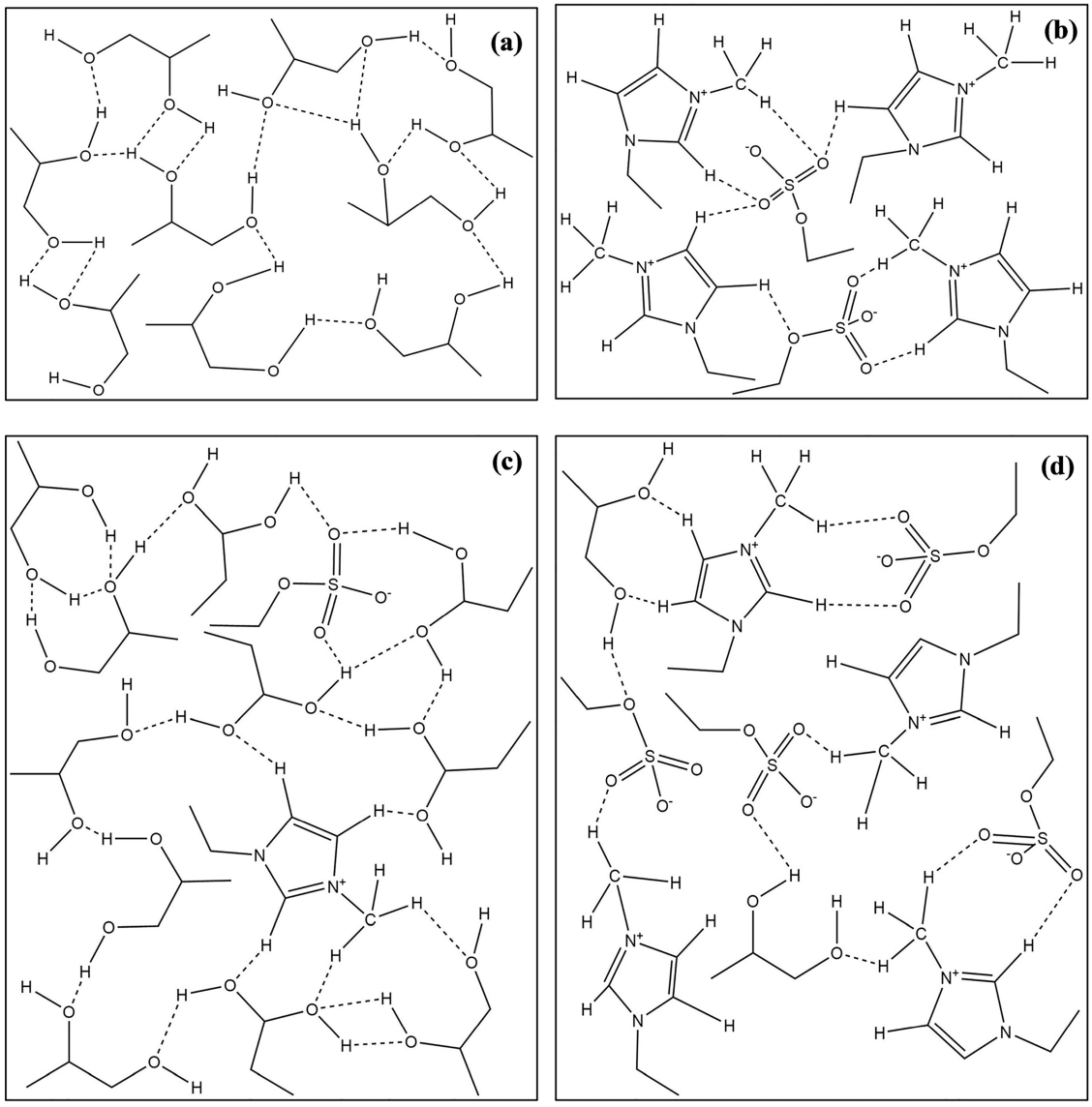

The NIR spectra of 0.4 $[C_2mim]C_2H_5SO_4$ mole fraction mixture is almost similar to that of 0.3 $[C_2mim]C_2H_5SO_4$ mole fraction. All the peak positions are the same as the former one except small blueshift of the peak at 6900 cm^{-1}. The synchronous 2D correlation contour plot shows nothing below 7000 cm^{-1}. This is because the spectral features are not changed much with temperature. The other features are similar to the former one. The PCA shows that PC1 is responsible for 92.08753% of the total spectral variation. The position of the peaks in the loading of PC1 is similar to that of 0.3 but scores linearly increase here. The PC2 is also similar to the former one.

As the mole fraction of $[C_2mim]C_2H_5SO_4$ increases, the peak at 6184 cm^{-1} becomes more intense and the peak at 6300 cm^{-1} diminishes. The reason for the increase in the intensity of the peak at 6184 cm^{-1} is the increasing number of this particular bond, and the vanishing of the peak at 6300 cm^{-1} suggests the breaking of the strong multiple hydrogen bonds to form weaker bonds. Another interesting feature of this binary mixture is that as the mole fraction of $[C_2mim]C_2H_5SO_4$ is increased, the position of the auto peak at 7000 cm^{-1} undergoes blueshift providing evidence of weakening on the intermolecular and intramolecular hydrogen bonds by the addition of $[C_2mim]C_2H_5SO_4$. The 2D synchronous and asynchronous contour plots, and the loadings and scores of the first four components are given in Figures S1−S18, and the eigenvalues and percentage of variance from the PCA are tabulated in Tables S4−S12.

The NIR spectral analysis of the pure propane-1,2-diol shows that in pure propane-1,2-diol intramolecular hydrogen bonding is dominating. Hence, the intermolecular hydrogen bonds are weaker here. However, the number of hydrogen bonds is higher. As the temperature increases, the intermolecular bonds weaken, and the hydrogen bonding structure is disrupted. When $[C_2mim]C_2H_5SO_4$ is added to propane-1,2-diol, the structure of the propane-1,2-diol is broken down. However, due to the domination of intramolecular hydrogen bonds, the molecular voids cannot be filled, increasing in

https://doi.org/10.1021/acsomega.3c03457
ACS Omega 2023, 8, 32690−32700

excess molar volume as discussed earlier. At lower content of $[C_2mim]C_2H_5SO_4$, the bonding is stronger resulting in the positive viscosity deviation. The smaller number of bonds between unlike molecules are also predicted in the excess molar Gibbs free energy plot, supported by the NIR spectra. The entropy also decreases with an increasing amount of $[C_2mim]C_2H_5SO_4$. At higher content of $[C_2mim]C_2H_5SO_4$, the intermolecular bonds between propane-1,2-diol molecules become insignificant and the expected amount of hydrogen bonding interaction is not formed due to the intervention from intramolecular bonds as observed from NIR analysis. At higher content of $[C_2mim]C_2H_5SO_4$, the excess molar volume becomes more positive, viscosity deviation becomes more negative, the excess molar Gibbs free energy is more negative, and activation entropy increases slightly due to the same reason. A visualization of the molecular-level interaction binary mixtures of $[C_2mim]C_2H_5SO_4$ and propane-1,2-diol and their pure components are given in Scheme 1.

CONCLUSIONS

In comparison to the pure components, the physicochemical properties of binary mixtures of $[C_2mim]C_2H_5SO_4$ and propane-1,2-diol differ significantly. The densities increase but viscosities decrease as the content of $[C_2mim]C_2H_5SO_4$ is increased in the mixture. The temperature dependence of viscosity follows non-Arrhenius behavior and is fitted well in VFT and mVFT equations. Excess molar volumes are positive but the other excess thermodynamic parameters are found to be negative for higher $[C_2mim]C_2H_5SO_4$ content. The values of Gibbs free energy of activation for viscous flow are all positive over the whole composition range indicating the non-spontaneity of the viscous flow and are increasing as the mole fraction of $[C_2mim]C_2H_5SO_4$ increases. The entropies are negative indicating the more ordered structure after flowing the liquid. The trends of enthalpy change are the same as those of entropy. The NIR spectral analysis shows that as the mole fraction of $[C_2mim]C_2H_5SO_4$ increases the intermolecular bonds between propane-1,2-diol molecules are broken down, some of the -OH groups form the solvated $[C_2mim]C_2H_5SO_4$ cations and anions, and some of the -OH groups become free from intermolecular hydrogen bonds and form intramolecular hydrogen bonds. It is thus the interplay between intermolecular and intramolecular hydrogen bonding that dictates the physicochemical properties of the IL with an alcohol.

ASSOCIATED CONTENT

Supporting Information

The Supporting Information is available free of charge at https://pubs.acs.org/doi/10.1021/acsomega.3c03457.

Fitted parameters (A, B, T_0) and corresponding fitting coefficient (R^2) of the various equations for the viscosities; coefficients of the Redlich−Kister equation (A_i); activation enthalpy and activation entropy of viscous flow of the binary system of $[C_2mim]C_2H_5SO_4$ and propane 1,2-diol at different temperatures; eigenvalues and percentage of variance for the principal components of the binary mixture of $[C_2mim]C_2H_5SO_4$ and propane-1,2-diol of 0.1001 to 0.8911$[C_2mim]$-$C_2H_5SO_4$ mole fraction; and synchronous and asynchronous 2D NIR correlation spectra calculated from the temperature-dependent spectral changes and loadings and scores for the PC1, PC2, PC3, and PC4 of the temperature-dependent NIR spectra of the binary mixture of $[C_2mim]C_2H_5SO_4$ and propane-1,2-diol at 0.1011−0.8911 $[C_2mim]C_2H_5SO_4$ mole fraction in the range of 6000−7500 cm^{-1} (PDF)

AUTHOR INFORMATION

Corresponding Author

Md. Abu Bin Hasan Susan − *Department of Chemistry and Dhaka University Nanotechnology Center (DUNC), University of Dhaka, Dhaka 1000, Bangladesh;* orcid.org/0000-0003-0752-1979; Email: susan@du.ac.bd

Author

Md. Ahad Ali − *Department of Chemistry, University of Dhaka, Dhaka 1000, Bangladesh; Department of Chemistry, Jashore University of Science and Technology, Jashore 7408, Bangladesh*

Complete contact information is available at: https://pubs.acs.org/10.1021/acsomega.3c03457

Notes

The authors declare no competing financial interest.

ACKNOWLEDGMENTS

The authors acknowledge Dhaka University to provide Article Publishing Charges under the International Publication Grant of Dhaka University. Bose Center for Advanced Study and Research in Natural Sciences is acknowledged for financial support. M.A.A. also acknowledges an NST Fellowship from the Ministry of Science and Technology, Bangladesh.

REFERENCES

(1) Freemantle, M. *An Introduction to Ionic Liquids*; RSC Publishing: Cambridge, UK, 2009.

(2) Angell, C. A.; Ansari, Y.; Zhao, Z. Ionic Liquids: Past, Present and Future. *Faraday Discuss.* **2012**, *154*, 9−27.

(3) Stalpaert, M.; Peeters, N.; de Vos, D. Conversion of Lactide to Acrylic Acid by a Phosphonium Ionic Liquid and Acid Cocatalyst. *Catal. Sci. Technol.* **2018**, *8*, 1468−1474.

(4) Yan, D.; Wang, G.; Gao, K.; Lu, X.; Xin, J.; Zhang, S. One-pot Synthesis of 2, 5-Furandicarboxylic Acid from Fructose in Ionic Liquids. *Ind. Eng. Chem. Res.* **2018**, *57*, 1851−1858.

(5) Wei; Wang, Y.; Chen, J.; Xu, P.; Zhou, Y. Preparation of Ionic Liquid Modified Magnetic Metal-Organic Frameworks Composites for The Solid-Phase Extraction of α−Chymotrypsin. *Talanta* **2018**, *182*, 484−491.

(6) Bogdanov, M. G.; Svinyarov, I. Efficient Purification of Halide-Based Ionic Liquids using Improved Apparatus for Continuous Liquid-Liquid Extraction. *Sep. Purif. Technol.* **2018**, *196*, 57−60.

(7) Rdzanek, P.; Marszalek, J.; Kaminski, W. Biobutanol Concentration by Pervaporation Using Supported Ionic Liquid Membranes. *Sep. Purif. Technol.* **2018**, *196*, 124−131.

(8) Zhang, L.; Shu, Z.; Yang, N.; Wang, B.; Dou, H.; Zhang, N. Improvement in Antifouling and Separation Performance of PVDF Hybrid Membrane by Incorporation of Room Temperature Ionic Liquids Grafted Halloysite Nanotubes for Oil−Water Separation. *J. Appl. Polym. Sci.* **2018**, *135*, 46278.

(9) Wilkes, J. S.; Levisky, J. A.; Wilson, R. A.; Hussey, C. L. Dialkylimidazolium Chloroaluminate Melts: A New Class of Room-Temperature Ionic Liquids for Electrochemistry, Spectroscopy and Synthesis. *Inorg. Chem.* **1982**, *21*, 1263−1264.

(10) Zhao, M.; Zheng, L.; Bai, X.; Li, N.; Yu, L. Fabrication of Silica Nanoparticles and Hollow Spheres Using Ionic Liquid Microemulsion Droplets as Templates. *Colloids Surf., A* **2009**, *346*, 229−236.

(11) Li, Z.; Zhang, J.; Du, J.; Han, B.; Wang, J. Preparation of Silica Microrods with Nano-Sized Pores in Ionic Liquid Microemulsions. *Colloids Surf., A* **2006**, *286*, 117−120.
(12) Moniruzzaman, M.; Kamiya, N.; Goto, M. Biocatalysis in Water-in-ionic Liquid Microemulsions: A Case Study with Horseradish Peroxidase. *Langmuir* **2009**, *25*, 977−982.
(13) Pavlidis, I. V.; Gournis, D.; Papadopoulos, G. K.; Stamatis, H. Lipases in Water-in-Ionic Liquid Microemulsions: Structural and Activity Studies. *J. Mol. Catal. B* **2009**, *60*, 50−56.
(14) Zheng, W.; Huang, K.; Wu, Y.; Hu, X. Protic Ionic Liquid as Excellent Shuttle of MDEA for Fast Capture of CO_2. *AIChE J.* **2018**, *64*, 209−219.
(15) Yang, X.; Song, H.; Wang, J.; Zou, W. Temperature and Composition Dependence of The Density, Viscosity and Refractive Index of Binary Mixtures of a Novel Gemini Ionic Liquid with Acetonitrile. *RSC Adv.* **2016**, *6*, 29172−29181.
(16) Tokuda, H.; Hayamizu, K.; Ishii, K.; Susan, M. A. B. H.; Watanabe, M. Physicochemical Properties and Structures of Room Temperature Ionic Liquids. 1. Variation of Anionic Species. *J. Phys. Chem. B* **2004**, *108*, 16593−16600.
(17) Tokuda, H.; Hayamizu, K.; Ishii, K.; Susan, M. A. B. H.; Watanabe, M. Physicochemical Properties and Structures of Room Temperature Ionic Liquids. 2. Variation of Alkyl Chain Length in Imidazolium Cation. *J. Phys. Chem. B* **2005**, *109*, 6103−6110.
(18) Tokuda, H.; Ishii, K.; Susan, M. A. B. H.; Tsuzuki, S.; Hayamizu, K.; Watanabe, M. Physicochemical Properties and Structures of Room Temperature Ionic Liquids. 3. Variation of Cationic Structures. *J. Phys. Chem. B* **2006**, *110*, 2833−2839.
(19) Pereiro, B. A.; Rodriguez, A. P. Thermodynamic Properties of Ionic Liquids in Organic Solvents from (293.15 to 303.15) K. *J. Chem. Eng. Data* **2007**, *52*, 600−608.
(20) AlTwaim, M. S.; Al-Jimaz, A. S.; Alkhaldi, K. H. A. E. Liquid Extraction of Toluene from Heptane, Octane or Nonane Using Mixed Ionic Solvents of 1-Ethyl-3- methylimidazolium Methylsulfate and 1-Hexyl-3-methylimidazolium Hexafluorophosphate. *J. Chem. Eng. Data* **2019**, *64*, 169−175.
(21) Garcıa-Miaja, G.; Troncoso, J.; Romanı, L. Excess Enthalpy, Density, And Heat Capacity for Binary Systems of Alkylimidazolium-based Ionic Liquids and Water. *J. Chem. Thermodyn.* **2009**, *41*, 161−166.
(22) Gonzalez, E. J.; Gonzalez, B.; Calvar, N.; Domınguez, A. Physical Properties of Binary Mixtures of the Ionic Liquid 1-Ethyl-3-Methylimidazolium Ethyl Sulfate with Several Alcohols at T = (298.15, 313.15, and 328.15) K and Atmospheric Pressure. *J. Chem. Eng. Data* **2007**, *52*, 1641−1648.
(23) Lehmann, J.; Rausch, M. H.; Leipertz, A.; Fröba, A. P. Densities and Excess Molar Volumes for Binary Mixtures of Ionic Liquid 1-Ethyl-3-Methylimidazolium Ethylsulfate with Solvents. *J. Chem. Eng. Data* **2010**, *55*, 4068−4074.
(24) Kiefer, J.; Molina, M. M.; Noack, K. The Peculiar Nature of Molecular Interactions between an Imidazolium Ionic Liquid and Acetone. *ChemPhysChem* **2012**, *13*, 1213−1220.
(25) Reddy, M. S.; Thomas, K.; Raju, S. S.; Nayeem, S. M.; Khan, I.; Krishana, K. B. M.; Babu, B. H. Excess Thermodynamic Properties for Binary Mixtures of Ionic Liquid 1-Ethyl-3-methylimidazolium Ethyl-Sulfate and 2-Methoxyethanol from T (298.15 to 328.15) K at Atmospheric Pressure. *J. Solution Chem.* **2016**, *45*, 675−701.
(26) Liu, Q.; Ma, L.; Wang, S.; Ni, Z.; Fu, X.; Wang, J.; Zheng, Q. Study on the properties of density, viscosity, excess molar volume, and viscosity deviation of $[C_2mim][NTf_2]$,$[C_2mmim][NTf_2]$,$[C_4mim]$-$[NTf_2]$, and $[C_4mmim][NTf_2]$ with PC binary mixtures. *J. Mol. Liq.* **2021**, *325*, No. 114573.
(27) Fu, X.; Wang, S.; Huang, Y.; Yang, X.; Liu, Q.; Zheng, Q. Densities and apparent molar volumes of diluent solutions of $[EmimNTf_2]$,$[BmimNTf_2]$, and $[BmmimNTf_2]$ in DEGDME and TEGDME. *J. Mol. Liq.* **2021**, *341*, No. 117328.
(28) Liu, Q.; Dai, H.; Chi, H.; Shi, K.; Zheng, Q.; Qi, Y. The density and dynamic viscosity for dilute solutions of $[Emim][NTf_2]$[Bmim]-$[NTf_2]$, and $[Bmmim][NTf_2]$ in ethylene glycol. *J. Mol. Liq.* **2023**, *371*, No. 121080.
(29) Fernandes, R. L.; Hoga, H. E.; Torres, R. B. Molecular interactions of ionic liquid {n-butylammonium methanoate (N_4Met)+ alcohols} at several temperatures: Thermodynamic and spectroscopic properties. *J. Chem. Thermodyn.* **2020**, *148*, No. 106140.
(30) Hoga, H. E.; Fernandes, R. L.; Olivieri, G. V.; Torres, R. B. Molecular interactions of (ionic liquid butylammonium methanoate+ alcohols) at several temperatures. Part II: sec-Butylammonium methanoate (S4Met). *J. Chem. Thermodyn.* **2023**, *178*, No. 106970.
(31) Masilo, K.; Bahadur, I. Intermolecular Interactions between 1-Ethyl-3-methylimidazolium-Based Ionic Liquids with Carboxylic Acid at Different Temperatures via Thermodynamic and Spectroscopic Studies. *J. Chem. Eng. Data* **2021**, *66*, 1211−1230.
(32) Ali, M. A.; Susan, M. A. B. H. Volumetric and Spectroscopic Studies of 1-ethyl-3-methylimidazolium Ethylsulfate/Propane-1-ol Binary Mixtures at Different Temperatures. *Spectr. Emerg. Sci.* **2022**, *2*, 17−28.
(33) Hofman, T.; Gołdon, A.; Nevines, A.; Letcher, T. M. Densities, excess volumes, isobaric expansivity, and isothermal compressibility of the (1-ethyl-3-methylimidazolium ethylsulfate+ methanol) system at temperatures (283.15 to 333.15) K and pressures from (0.1 to 35) MPa. *J. Chem. Thermodyn.* **2008**, *40*, 580−591.
(34) Gómez, E.; González, B.; Calvar, N.; Tojo, E.; Domínguez, Á. Physical properties of pure 1-ethyl-3-methylimidazolium ethylsulfate and its binary mixtures with ethanol and water at several temperatures. *J. Chem. Eng. Data* **2006**, *51*, 2096−2102.
(35) Fröba, A. P.; Kremer, H.; Leipertz, A. Density, refractive index, interfacial tension, and viscosity of ionic liquids $[EMIM][EtSO_4]$, $[EMIM][NTf_2]$,$[EMIM][N(CN)_2]$, and $[OMA][NTf_2]$ in dependence on temperature at atmospheric pressure. *J. Phys. Chem. B* **2008**, *112*, 12420−12430.
(36) Zarei, H.; Golroudbari, S. A.; Behroozi, M. Experimental studies on volumetric and viscometric properties of binary and ternary mixtures of N, N-dimethylacetamide, N-methylformamide and propane-1, 2-diol at different temperatures. *J. Mol. Liq.* **2013**, *187*, 260−265.
(37) Cano-Gómez, J. J.; Iglesias-Silva, G. A.; Cortez-Sánchez, L. D.; Castillo-Escobedo, M. T. Densities and Viscosities for Binary Liquid Mixtures of Butan-1-ol+ Propane-1, 2-diol + Butane-1, 2-diol and 2-Methylpropan-1-ol+ Propane-1, 2-diol,+ Butane-1, 2-diol from 298.15 to 333.15 K at 0.1 MPa. *J. Chem. Eng. Data* **2017**, *62*, 4252−4265.
(38) Doghaei, A. V.; Rostami, A. A.; Omrani, A. Densities, viscosities, and volumetric properties of binary mixtures of 1, 2-propanediol+ 1-heptanol or 1-hexanol and 1, 2-ethanediol+ 2-butanol or 2-propanol at T=(298.15, 303.15, and 308.15) K. *J. Chem. Eng. Data* **2010**, *55*, 2894−2899.
(39) Anwar, N.; Riyazuddeen. Effect of composition and temperature variations on thermophysical properties of binary and ternary mixtures of 1-ethyl-3-methylimidazolium ethylsulfate with 1-butanol and/or methanol. *Fluid Phase Equilib.* **2017**, *437*, 127−139.
(40) Arce, A.; Rodil, E.; Soto, A. Volumetric and viscosity study for the mixtures of 2-ethoxy-2-methylpropane, ethanol, and 1-ethyl-3-methylimidazolium ethyl sulfate ionic liquid. *J. Chem. Eng. Data* **2006**, *51*, 1453−1457.
(41) Živković, E.; Kijevčanin, M.; Radović, I.; Šerbanović, S. P. Viscosities and refractive indices of binary systems acetone+ 1-propanol, acetone+ 1, 2-propanediol and acetone+ 1, 3-propanediol. *Chem. Ind. Chem. Eng. Quart.* **2014**, *20*, 441−455.
(42) Zafarani-Moattar, M. T.; Shekaari, H. Volumetric and Speed of Sound of Ionic Liquid, 1-butyl-3-methylimidazolium Hexafluorophosphate with Acetonitrile and Methanol at T = (298.15 to 318.15) K. *J. Chem. Eng. Data* **2005**, *50*, 1694−1699.
(43) Wang, J.; Tian, Y.; Zhao, Y.; Zhuo, K. A Volumetric and Viscosity Study for the Mixtures of 1-N-Butyl-3-Methylimidazolium Tetrafluoroborate Ionic Liquid with Acetonitrile, Dichloromethane, 2-Butanone And *N N*-Dimethylformamide. *Green Chem.* **2003**, *5*, 618−622.

https://doi.org/10.1021/acsomega.3c03457
ACS Omega 2023, 8, 32690−32700

(44) González, E. J.; Alonso, L.; Domínguez, Á. Physical Properties of Binary Mixtures of the Ionic Liquid 1-Methyl-3-octylimidazolium Chloride with Methanol, Ethanol, and 1-Propanol at T = (298.15, 313.15, and 328.15) K and at P = 0.1 MPa. *J. Chem. Eng. Data* **2006**, *51*, 1446−1452.
(45) Vogel, D. H. Das Temperatur-abhaengigkeitsgesetz der Viskositaet von Fluessigkeiten. *Phys. Z.* **1921**, *22*, 645.
(46) Fulcher, G. S. Analysis of Recent Measurements of the Viscosity of Glasses. *J. Am. Ceram. Soc.* **1925**, *8*, 339−355.
(47) Tammann, G.; Hesse, W. Die Abhängigkeit der Viscosität von der Temperatur bie unterkühlten Flüssigkeiten. *Z. Anorg. Allg. Chem.* **1926**, *156*, 245−257.
(48) Mauro, J. C.; Yueb, Y.; Ellisona, A. J.; Guptac, P. K.; Allana, D. C. Viscosity of Glass-Forming Liquids. *Proc. Natl. Acad. Sci. U. S. A.* **2009**, *106*, 19780−19784.
(49) Redlich, O.; Kister, A. T. Algebraic Representation of Thermodynamic Properties and the Classification of Solutions. *Ind. Eng. Chem.* **1948**, *40*, 345−348.
(50) Tokuda, H.; Tsuzuki, S.; Susan, M. A. B. H.; Hayamizu, K.; Watanabe, M. How Ionic Are Room-Temperature Ionic Liquids? An Indicator of the Physicochemical Properties. *J. Phys. Chem. B* **2006**, *110*, 19593−19600.
(51) Kapadi, U. R.; Hundiwale, D. G.; Patil, N. B.; Lande, M. K.; Patil, P. R. Studies of Viscosity and Excess Molar Volume of Binary Mixtures of Propane-1,2-diol with Water at Various Temperatures. *Fluid Phase Equilib.* **2001**, *192*, 63−70.
(52) Anouti, M.; Vigeant, A.; Jacquemin, J.; Brigouleix, C.; Lemordant, D. Volumetric Properties, Viscosity and Refractive Index of the Protic Ionic Liquid, Pyrrolidinium Octanoate, in Molecular Solvents. *J. Chem. Thermodyn.* **2010**, *42*, 834−845.
(53) Workman, Jr., J.; Weyer, L. *Practical Guide and Spectral Atlas for Interpretive Near-Infrared Spectroscopy*; CRC Press, 2007.
(54) Noda, I.; Ozaki, Y. *Two-dimensional Correlation Spectroscopy − Applications in Vibrational and Optical Spectroscopy*; John Wiley & Sons Ltd., 2004.
(55) Haufa, K. Z.; Czarnecki, M. A. Effect of Temperature and Water Content on The Structure of 1,2-Propanediol and 1,3-Propanediol: Near-Infrared Spectroscopic Study. *Vib. Spectrosc.* **2009**, *51*, 80−85.

https://doi.org/10.1021/acsomega.3c03457
ACS Omega 2023, 8, 32690−32700